Soft Matter

Particle anisotropy tunes emergent behavior in active colloidal systems

Journal:	*Soft Matter*
Manuscript ID	SM-ART-05-2020-000913.R1
Article Type:	Paper
Date Submitted by the Author:	15-Dec-2021
Complete List of Authors:	Moran, Shannon; University of Michigan, Chemical Engineering Bruss, Isaac; University of Michigan, Chemical Engineering Shoenhofer, Philip; University of Michigan, Chemical Engineering Glotzer, Sharon; University of Michigan, Chemical Engineering

Soft Matter

ARTICLE TYPE

Cite this: DOI: 10.1039/xxxxxxxxxx

Particle anisotropy tunes emergent behavior in active colloidal systems†

Shannon E. Moran,[a] Isaac R. Bruss,[a] Philipp W. A. Schönhöfer,[a] and Sharon C. Glotzer[ab]‡

Received Date
Accepted Date

DOI: 10.1039/xxxxxxxxxx

www.rsc.org/journalname

Studies of active particle systems have demonstrated that particle anisotropy can impact the collective behavior of a system, motivating a systematic study. Here, we report a systematic computational investigation of the role of anisotropy in shape and active force director on the collective behavior of a two-dimensional active colloidal system. We find that shape and force anisotropy can combine to produce critical densities both lower and higher than those of disks. We demonstrate that changing particle anisotropy tunes what we define as a "collision efficiency" of inter-particle collisions in leading to motility-induced phase separation (MIPS) of the system. We use this efficiency to determine the relative critical density across systems. Additionally, we observe that local structure in phase-separated clusters is the same as the particle's equilibrium densest packing, suggesting a general connection between equilibrium behavior and non-equilibrium cluster structure of self-propelled anisotropic particles. In engineering applications for active colloidal systems, shape-controlled steric interactions such as those described here may offer a simple route for tailoring emergent behaviors.

1 Introduction

Active matter is a field of rapidly expanding interest and research activity over the last decade [1–4]. Vicsek's pioneering work showed a collection of point particles with alignment rules displays rich collective behavior, including phase separation [5]. However, theoretical work describing the collective behavior of bacteria demonstrates that phase separation behavior is not reliant upon explicit alignment rules [6]. In a phenomenon known as "motility-induced phase separation" (MIPS), systems of disks were found to phase separate as a consequence of density-dependent particle velocity [7]. This phase separation behavior of isotropic particles has been explained using a variety of models, including: athermal phase separation [8], the kinetic steady-state balancing of particle fluxes [9,10], classical nucleation [11,12], and the balancing of collision and ballistic timescales [13]. Importantly, phase separation predicted by theory has been observed in experiments, which confirm the activity-dependent formation of clusters and "active crystals" [14–16].

However, in real-world systems particles (e.g. bacteria) are rarely isotropic in shape. Thus, one thrust in the active matter community has focused on understanding how particle anisotropy will change the behavior theoretically predicted for systems of isotropic particles. In a simple anisotropic model, simulations of rods with varying aspect ratios and densities display a rich variety of collective motion, such as laning, swarming, and jamming [17–19]. Additionally, simply changing the direction of the driving force relative to a fixed particle shape (e.g. "rough" triangles) drastically alters the resulting collective behavior and onset of phase separation [20,21].

Few general mechanisms have been proposed for the varying impacts of particle anisotropy on collective behavior. Active squares display a steady state "oscillatory" regime in which large clusters break up and re-form [22]. A combination of activity and molecule shape has shown to enhance polymerization [23]. Mixtures of gear-shaped "spinners" with opposite rotational driving forces phase separate through competing steric interactions [24–26]. In systems of active "dumbbells", particle anisotropy allows for the stabilization of cluster rotation [27,28]. This cluster rotation is also observed in active squares [22], but is notably absent in clusters of frictionless isotropic particles.

From these studies, we can see a general description of the impact of particle shape anisotropy on emergent system behavior is needed. Such a description would allow us to tailor the form and onset of critical behavior in active systems through "implicit" steric means, rather than explicit interaction rules.

In this paper we aim to develop a generalized description of the role of active particle anisotropy through direct comparison to frictionless active disks (i.e. isotropic particles). We study a family of translationally self-propelled 2D polygons (of side num-

[a]Department of Chemical Engineering, University of Michigan, Ann Arbor, MI 48109
[b]Biointerfaces Institute, University of Michigan, Ann Arbor, MI 48109

† Electronic Supplementary Information (ESI) available: [details of any supplementary information available should be included here]. See DOI: 10.1039/cXsm00000x/

‡ Additional footnotes to the title and authors can be included *e.g.* 'Present address:' or 'These authors contributed equally to this work' as above using the symbols: ‡, §, and ¶. Please place the appropriate symbol next to the author's name and include a `\footnotetext` entry in the the correct place in the list.

ber $3 \leq n \leq 8$) with force director anisotropy implemented as shown in Figure 1. This choice of shapes systematically extends previous studies on triangles with inertia[20], triangles with friction[21], and squares[22]. Full simulation parameters and additional details can be found in Section 2.

We show that the onset of phase separation at a critical density ϕ^* is highly dependent on the shape of the particle given a constant Péclet (Pe) number, where Pe is a measure of active (advective) to diffusive motion. In our system, we observe phase separation at densities as low as $\phi^* = 0.01$ in vertex-forward 6-gons, or as high as $\phi^* = 0.37$ in edge-forward 3-gons– both below and above ϕ^* of disks. Interestingly, we find that the direction of the force director is sufficient for changing the ϕ^* for a given shape, but not for changing the relative phase separation onset between different shapes. Specifically, edge-forward active particles have higher ϕ^* than their vertex-forward counterparts. Additionally, the internal structure of the phase-separated cluster is primarily determined by the particle shape and resembles each shape's equilibrium densest packing. This resemblence suggests a link between structure and critical density not yet explored in active systems.

In addition to this systematic study, this work's contribution to the study of anisotropic active matter is the introduction of a "collision efficiency" measure. We find that systems with the lowest critical densities are also those that maximize particle deceleration per unit increase in inter-particle collision pressure, P_{coll}. That is, some shapes can more efficiently convert particle collisions into decreases in particle velocity, v, leading to phase separation. This allows us to quantitatively attribute changes to ϕ^* in systems of shapes versus disks to steric impacts on collisions, and directly shows that we can tune critical behavior of active systems by tuning the nature of the inter-particle collision dynamics.

We note that 3- and 4-gons (the only two previously studied active polygons) behave fundamentally differently from other polygons. We attribute this to the slip planes present in their densest packings. As these shapes have been used as model systems for a number of previous studies[20–22], we show why such results should not be generalized to systems that do not have slip planes.

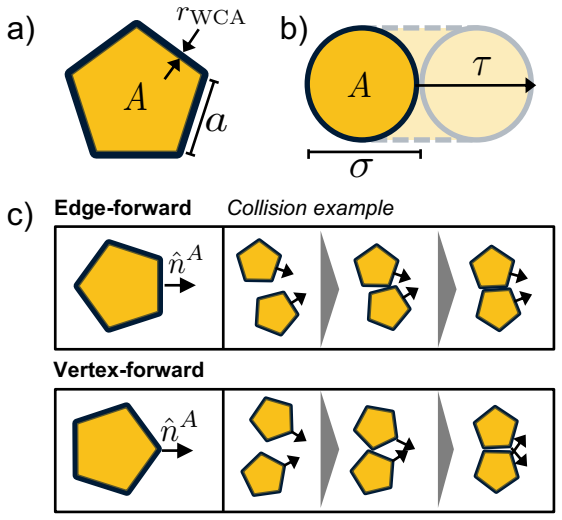

Fig. 1 (a) Shape anisotropy is studied with a family of regular polygons of side length a. Here we show a pentagon as example. Particles interact through a purely repulsive WCA potential characterized by r_{WCA}. Full specification can be found in Section 2. (b) Simulation timescales are characterized by τ, the time for a particle to ballistically travel its characteristic length, σ, calculated as the diameter of an equiarea (A) disk. (c) Force anisotropy is defined by the active force director, $\hat{n}^A$, which propels the shape either edge- or vertex-forward. A key feature of this system is that collisions of anisotropic particles can sustain translational and/or rotational motion. Illustrative collisions are provided for each force director.

2 Methods

2.1 Model and dynamics

The model particles used in this study are shown in Figure 1. We study a family of regular polygons of side number $3 \leq n \leq 8$. We set particle side length a to maintain a constant side-to-corner perimeter ratio, ζ, to $\zeta = \frac{\sum_s a_s}{2\pi r_{\text{WCA}}} = 9$ over all sides s. Here, $2\pi r_{\text{WCA}}$ is the corner rounding introduced by the frictionless, purely repulsive, excluded volume Weeks-Chandler-Anderson (WCA) potential of interaction length r_{WCA}, which we set equal to 1 for all shapes under study to keep the interaction length consistent. The WCA potential is a shifted Lennard-Jones potential, shifted to zero and cut off at its minimum. Mathematically, the interaction between particles i and j is constructed as $U(r_{ij}) = 4\varepsilon[(\sigma_{\text{WCA}}/r_{ij})^{12} - (\sigma_{\text{WCA}}/r_{ij})^6] + \varepsilon$ for $r \leq r_{\text{cut}}$ and 0 for $r > r_{\text{cut}}$ where $r_{\text{cut}} = 2^{(1/6)}\sigma_{\text{WCA}}$ and $\sigma_{\text{WCA}} = 2r_{\text{WCA}}$[29].

We know from equilibrium studies[30–32] and other works on active anisotropic particle systems[22] that self assembly and critical behavior is sensitive to the effective "roundness" of particle vertices. As the repulsive interaction introduces a slight "rounding" to the shapes, maintaining a constant ζ over all simulations ensures our systems can be compared with one another. This value $\zeta = 9$ was chosen to balance shape fidelity (less rounding) and simulation feasibility with computational demands.

We also explore anisotropy in the constant active force director ($\boldsymbol{F}_i^A = v_0 \hat{n}_i^A(\cos\theta_i, \sin\theta_i)$) applied to each particle i. For a given simulation, we set $\hat{n}_i$ to be either perpendicular to a side of the particle (*edge-forward*) or bisecting a vertex (*vertex-forward*), as shown in Figure 1c. The active force director $\hat{n}_i$ is initialized randomly for each particle from the set of possible vertex-forward or edge-forward directions for each simulation, and is locked in the particle's frame of reference. The active force direction changes only with particle rotation due to thermal fluctuations and collisions.

We took further care to ensure consistent anisotropy through our choice of active force magnitude and temperature. Our systems were run at Péclet (Pe) number of Pe = 150, where Pe is a measure of active (advective) to diffusive motion ($\text{Pe} = \frac{v_0\sigma}{k_B T}$, where σ is the diameter of an equi-area disk for a given shape). In this Pe regime, we can treat the active driving force as the primary contributor to particle motion over thermal fluctuations. By setting the temperature of the thermal bath governing the fluctuations to $k_B T = \frac{v_0\sigma}{\text{Pe}}$ and the magnitude of the active driving force

$v_0 = 1$, we ensure that the interaction distance between interacting particles remains constant for all simulations.

Particle motion was solved for using the Langevin equations of motion.

$$m_i \dot{\boldsymbol{v}}_{\boldsymbol{i}} = \sum_j \boldsymbol{F}_{ij}^{Ex} - \gamma \cdot \boldsymbol{v}_{\boldsymbol{i}} + \boldsymbol{F}_i^A + \boldsymbol{F}_i^R \quad (1)$$

$$m_i \ddot{\theta}_i = \sum_j \boldsymbol{T}_{ij}^{Ex} - \gamma_R \cdot \boldsymbol{\omega}_{\boldsymbol{i}} + \sqrt{2\mathscr{D}_{\mathscr{R}}}\eta(t)_i^R \quad (2)$$

Mass (m_i) is set to 1×10^{-2} such that the dynamics closely approximate the Brownian limit in line with the expected dynamics of bacteria and colloidal-scale particles. The forces and torques due to excluded volume ($\boldsymbol{F}_{ij}^{Ex}$ and $\boldsymbol{T}_{ij}^{Ex}$) were calculated using a discrete element method[33], which calculates interparticle interactions between a point on one particle perimeter and a point on another particle's perimeter. Translational and rotational velocities are given by v_i and ω_i, respectively. We parametrized the implicit solvent via the translational drag coefficient $\gamma = 1$ and $\gamma_R = \frac{\sigma^3\gamma}{3}$ per the Stokes-Einstein relationship. These parameter choices correspond to the overdamped, diffusive limit. Our model does not account for solvent-mediated hydrodynamic interactions between active particles. Although there is a small inertial component in our model, we confirmed that it is not critical for any of the observed behavior. The last term in both equations accounts for thermal fluctuations. Noise is included via Gaussian random forces $\boldsymbol{F}_i^R = \sqrt{2\gamma k_B T}\eta(t)$ that model a heat bath at temperature T. Here $\eta(t)$ are normalized zero-mean white-noise Gaussian processes ($\langle \eta_i(t) \rangle = 0$ and $\langle \eta_i(t)\eta_j(t') \rangle = \delta_{ij}\delta(t-t')$). This ensures thermodynamic equilibrium in the absence of the externally applied forces ($\boldsymbol{F}_{ij}^A$). The simulation protocol is described in Appendix A.1.

3 Results and Discussion

3.1 Phase separation and critical behavior

Figure 2a shows the critical density ϕ^* based on the occurrence of two density peaks in the local density distributions (for an in-depth description see Appendix A.2) for different regular polygons. As we increase the number of vertices (i.e. become more "disk-like"), we expected to see monotonically increasing critical density[34] from high-anisotropy 3-gons towards lower anisotropy 8-gons.

Instead phase-separation behavior does not vary monotonically with n. For shapes of $n = [3,4]$, we observe a ϕ^* near that of disks in this Pe regime, with exact value dependent on the force director. As we increase n to 5, we see a sharp decrease in ϕ^* with continued dependence on the force director. The lowest critical densities are observed for shapes of $n = 6$, above which we observe the expected monotonic increase in ϕ^* as n is increased to [7,8].[35]

We first address the impact of the force director. We expect ϕ^* to depend on the nature of the active force director because the stability of small cluster depends on the force directors, as suggested in the collision example diagram in Figure 1. Specifically, for vertex-forward shapes, the only stable dimer sustains translational motion. For edge-forward shapes, stable dimers exist that are either stationary and/or can sustain translational mo-

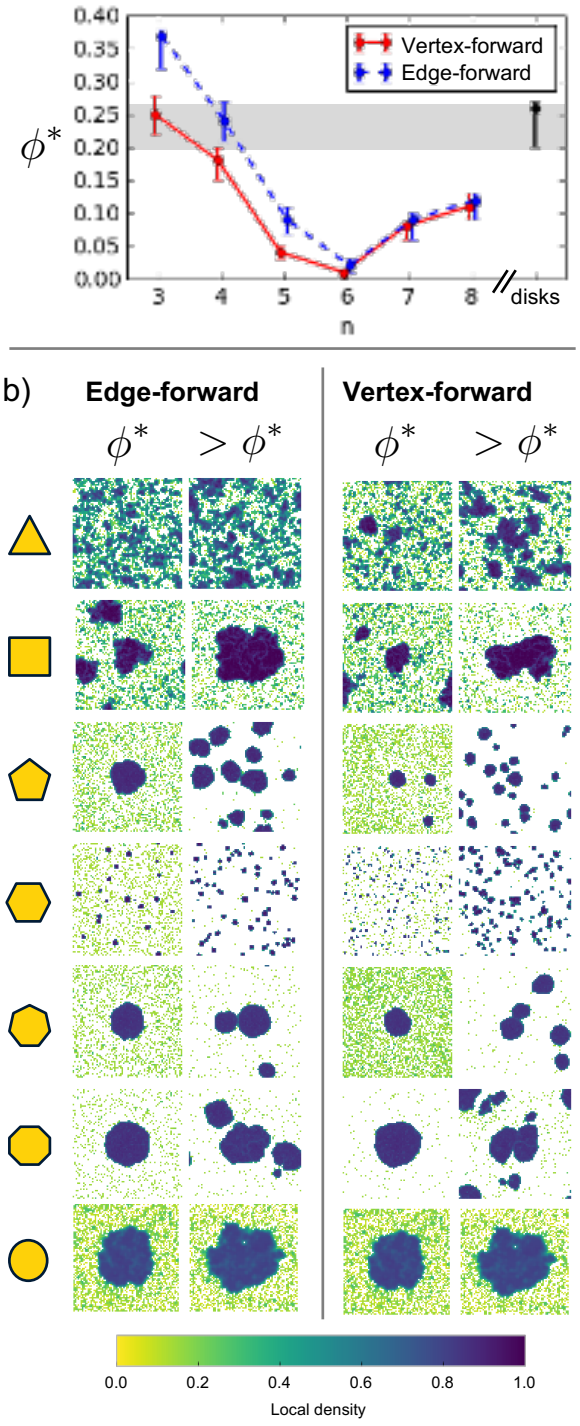

Fig. 2 Critical density and collective behavior of active anisotropic systems. (a) Critical density for systems of each n-gon. We define the critical density, ϕ^*, as the density at which $> 50\%$ of the replicates phase separate into clusters. Lower error bar bounds indicate the minimum system ϕ at which at least one replicate phase separated into clusters, while the upper error bar bounds indicate the minimum ϕ at which all replicates clustered. See also Appendix A.2. (b) Representative steady-state local density snapshots in the critical (ϕ^*) and phase separated ($> \phi^*$) regimes of edge forward (left) and vertex forward (right) active polygons. A distinctive feature of phase separation in systems of anisotropic particles is the formation of multiple stable clusters that persist for long time scales.

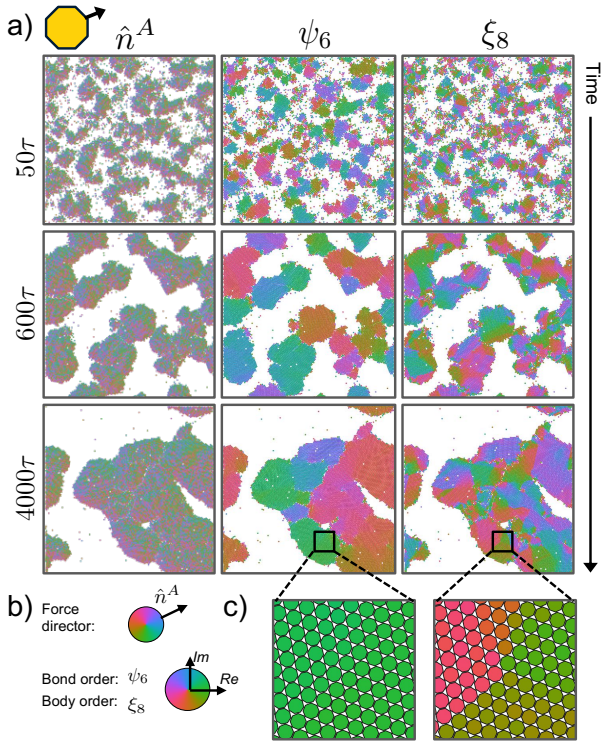

Fig. 3 Example of structural evolution of clusters in system of vertex-forward 8-gons at $\phi = 0.5$. a) Left column: Active force director $\hat{n}^A$ exhibits strong polarization at all times, pointing towards the center of the cluster both at the boundary and throughout the cluster. Center column: Hexatic bond order ψ_6 (see definition in Appendix A.3) forms quickly and uniformly through clusters. Spatial boundaries in the order parameter are the result of cluster mergers that have not yet annealed. Right column: Body order ξ_8 (see definition in Appendix A.3) accounts for particle orientation in the cluster. Strong orientational grains form in the clusters, though they do not span clusters as completely as bond order. Grain boundaries are apparent and do not anneal completely. b) Legend for orientation maps in (a). c) Snapshots of bond and body order from regions highlighted in (a).

tion. Looking only at the mechanical force balance on configurations of edge- versus vertex-forward particle clusters, we might expect that edge-forward particles would phase separate more easily due to more effective inter-particle slowing. However, the sustained translational motion of small clusters allows increased inter-cluster collisions in the vertex-forward systems. It is clear that this increased inter-cluster collision phenomena wins out, with lower ϕ^* for vertex forward $n = [3,4,5]$. Following this logic, the translational speed of a vertex-forward dimer relative to the particle ballistic velocity should decrease with increasing n. We hypothesize that for $n > 6$, this decrease in small cluster translational speed leads to the lack of difference between edge- and vertex-forward ϕ^*. Representative small-N clusters are shown for each combination of n-gon and force director in the Supplementary Information.

In investigating the structures formed by particles in the phase-separated cluster, we find that without exception the particles have assembled into their densest packing, as shown in the far right column of Figure 2b. Using this information, we make the following observations. For 6-gons (the shape with the lowest ϕ^*), the densest packing has neither void space nor slip planes. For 5-, 7-, and 8-gons, the densest packing has void space, but no slip planes. For 3- and 4-gons, the densest packing has no void space, but has slip planes. This leads us to hypothesize that a system's ability to inhibit particle movement in the cluster (where void space and slip planes play a role) is critical to understanding the critical behavior.

Additionally, the only two shapes in our simulations that exhibit an "oscillatory" regime in their phase behavior are 3- and 4-gons (videos available in the Supplemental Information). These shapes are also the only two that have slip planes in their densest packings. In the literature, other studies have noted oscillation as novel behavior accessed via anisotropy and activity[22,36]. We posit that the oscillatory regime for anisotropic particles is in fact a natural consequence of the preferred steady-state structure of the component particle shapes in these systems. We will revisit this claim more rigorously in Section 3.3.

Our final observation on the critical behavior is that the nature of the phase separation varies significantly based on shape, as shown in Figure 2b. Beyond the critical regime, we see the formation of many stable clusters at steady state for $n \geq 5$. This is in contrast to systems of isotropic disks, where secondary cluster formation is short-lived with phase separation characterized by a single large cluster[9,10]. The phenomena of multiple phase-separated clusters at steady state is theoretically predicted in bacteria[6], but not in other theoretical models focused on isotropic active particle phase separation[8,12].

3.2 Cluster growth and coarsening dynamics

It remains an open question in the literature as to how shape may affect the kinetics of phase separation, e.g. coarsening and domain growth laws in active systems. Here, we investigate how particle shape enables the observed phase separation initially into multiple small clusters with coarsening at steady state.

Before phase separating, systems exhibit localized areas of high-density fluctuations, as described in many other theoretical studies of active systems[7,8]. These localized areas of high density are hexagonally ordered, with the exception of 4-gons, which order on a square lattice. Following this initial structuring, orientational order develops consistent with the known densest packing of each regular polygon[37]. An example of this phase separation process in vertex-forward 8-gons is shown in Figure 3.

This transition from random orientation to close-ordered densest packing is due to the active collision pressure on the clusters. Studies on active disk cluster nucleation have confirmed that inward-pointing particles at the cluster boundary is a necessary condition for nucleation[11,12]. Similarly, active polygon clusters possess a net-inward force (Figure 3a). However, unlike in clusters of disks, the rotation of n-gons within the cluster is sterically inhibited. Thus, there exists a sustained inward-facing pressure on the clusters driving the structure to a densest packing.

We observe that the nature of the phase separation dynamics for shapes resembles that of quenched disks[10] for $n \geq 5$, as seen in Figure 2b. Multiple small clusters form and are stable at steady

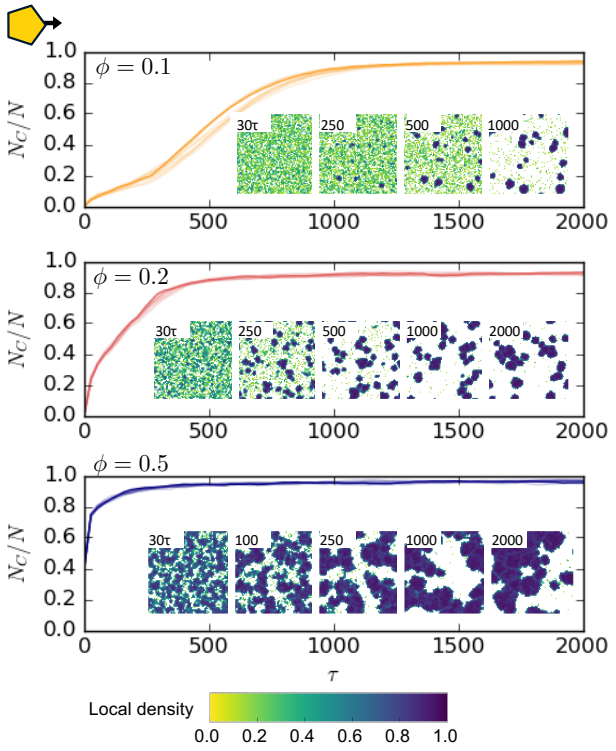

Fig. 4 Example of clustering (phase separation) kinetics for vertex-forward 5-gons at three system densities ($\phi > \phi^*$). The fraction of system particles in a cluster, N_C/N, is plotted over the evolution of the simulation. Particles are considered "in a cluster" if their local density is ≥ 0.6. N_c/N trajectories for all ten replicates for each ϕ are shown, though the behavior is so similar that the replicates are only distinguishable for $\phi = 0.1$. Snapshots are colored by local density, colorbar shown.

state (where steady state is determined by the methods described in Section 2). However, the coarsening behavior between shapes differs. As seen in Fig. 2, the critical-regime onset phase separation for $n = [5,7,8]$ is characterized by the formation of one (or few) clusters that quickly form and slowly grow, while for $n = 6$, cluster nucleation is so favorable that we see the nucleation of many small clusters even in the critical regime.

We demonstrate this coarsening behavior in Figure 4, where the fraction of the system in a cluster (N_C/N) is plotted over time (in units of τ, where τ is the time for a particle to ballistically travel its own diameter). At low densities, but even at those above the critical system density for a given shape, we observe rapid nucleation and growth of small clusters, which remain stable at steady state (this behavior is also observed in the low density/activity limit of dumbbells[27]). At higher densities, the size of the clusters increases the likelihood of another cluster colliding with it and merging to make a larger cluster.

This leads us to another key aspect of anisotropic systems not seen in disks: sustained rotational and translational motion of clusters (Figure 5). Previous studies on squares found that sustained motion drove the system into an oscillatory behavior[22]. We find that such motion is also critical to the coarsening of clusters of active shapes. In contrast, clustered disks cannot sustain motion, and quenched systems coarsen through the dissolution of some clusters and growth of others rather than inter-cluster collisions. The only net motion within clusters of disks is at the boundaries, where a balance of particle fluxes in/out characterizes the steady state configuration[10]. As a result, the steady state of multiple small clusters in a system of isotropic particles is unfavorable, as clusters in such systems are only stabilized by particles being self-propelled into the cluster.

3.3 Collision efficiency

Phase separation due to MIPS is the result of particle slowing as local density increases, with $v(\rho)$[7]. Here, we demonstrate a method for quantifying the impact of shape on $dv/d\rho$.

To build our intuition for this approach: at a particle level, we can describe MIPS as collision-induced slowing. In a system of frictionless disks, collisions between small numbers of particles are not stable, with clusters of small size ($n_C < 10$) generally having a short lifespan ($< \tau$). (Nucleation in disk systems is facilitated by local polarization of the active force directors leading to a stable nucleation seed[11,12].) In contrast, collisions between anisotropic particles can create long-lasting clusters of small n_C, "seeds", such as those highlighted in the Supplementary Information, Figure 1. In addition to lifetimes lasting $\gg \tau$, some seeds can sustain translational motion and/or stabilize collisions from external particles. While these seeds are not a necessary condition for phase separation, they facilitate the process by slowing both constituent seed particles and single particles colliding with the seed, leading to localized areas of high density.

At a system level, we can translate this collision-induced slowing to a "collision efficiency" during the nucleation and growth of clusters. We hypothesize that those systems in which collision work is more efficiently transformed into a decrease in average particle velocity (i.e. greater $-dv/d\rho$) are also those that are able to phase separate at lower system densities (lower ϕ^*). As the system density ϕ is a proxy for the number of collisions a particle experiences[13], particles with higher collision efficiency need fewer collisions– and thus lower ϕ– to reduce the average particle speed and lead to phase-separation of the system.

To demonstrate this quantitatively, we measure the instantaneous pressure P_{coll} due to inter-particle collisions (calculations detailed in Section A.4). In Figure 6a, we plot the trajectories of systems through v/P_{coll} space. We find that each system type (n and force direction) falls onto a well-defined trajectory with short nucleation, long growth, and flat steady-state regions. The slope of this growth regime, $-dv/d\rho$, is what we term the "collision efficiency". We observe that relative slopes of the growth regimes correctly predict the relative critical densities of the shapes studied, including the relative critical densities of edge-forward and vertex-forward systems of the same shape.

Notably, 3- and 4-gons require significantly higher collision pressure to reach steady state, as shown in Figure 6b. These systems fall on the same master curve, suggesting that some feature similarity in the system drives similarity in v/P_{coll} space. Using the concept of collision efficiency, we can now quantitatively demonstrate how the slip planes observed in 3- and 4-gon densest packings lead to the "oscillatory" behavior discussed

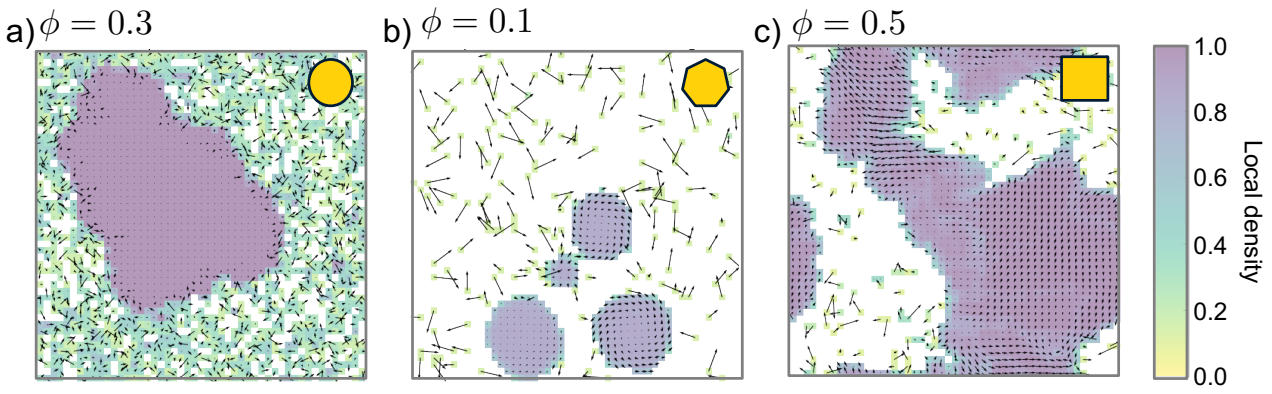

Fig. 5 Particle displacement fields for simulations at steady state, laid over a map of local densities. (a) Clusters of disks have no net motion, with particle motion limited to the cluster boundaries and gas phase. (Shown is a system of disks at $\phi = 0.3$). In contrast, clusters of anisotropic particles display both (b) net rotational motion (shown for edge-forward 7-gons, $\phi = 0.1$) and (c) net translational motion (shown for vertex-forward 4-gons, $\phi = 0.5$).

earlier and observed in previous works[22]. As shown in Figure 6c, systems of shapes whose densest packings do not have slip planes (like the edge-forward 5-gons shown) proceed monotonically through v/P_{coll} space with τ, eventually resulting in phase separation. In contrast, systems with slip planes do **not** proceed through v/P_{coll} space monotonically with τ. In the system shown of vertex-forward 3-gons, a phase-separating system proceeds through v/P_{coll} space as the phase-separated clusters form. At high P_{coll}, however, the system is no longer able to sustain the inter-particle collision pressure and the cluster breaks apart, retracing its path through v/P_{coll}. Additionally, the lack of hysteresis in this path through v/P_{coll} space during cluster dissolation confirms that this oscillatory phenomenon is not path dependent or a function of simulation protocol, but rather a function of the particle anisotropy alone. The oscillatory regime can be described as a system's inability to stabilize the inter-particle collision pressure.

In collision efficiency, we have introduced a metric that quantitatively explains how shape impacts the critical density in active systems. This framework tells us that we can tune the critical behavior of a system by altering how efficiently particles decelerate other particles in collisions.

4 Conclusions

In this work, we investigated the critical phase behavior of a 2D active matter system of anisotropic particles in which anisotropy was implemented through polygon shape and active force director. We demonstrated that we can quantitatively describe the critical behavior as a function of "collision efficiency", which can be tuned by engineering particle interactions (here, we explore only shape). Further, we observe that this critical behavior is related to the structure of the component particle shapes' densest packing at equilibrium.

We showed that increasing the efficiency of inter-particle collisions in slowing particles down during cluster growth is a key driver of decreasing critical densities. This observation is closely related to a number of theoretical developments in the field of active matter. We can think of this efficiency as a determinable scaling coefficient on the change in particle velocity with local density ($dv/d\rho$) in MIPS[6]. Similarly, an analytical determination of the average collision time for an inter-particle collision would allow prediction of critical onset through the balancing of $\tau_{\text{collision}}$ and $\tau_{\text{ballistic}}$ timescales[13]. Such an analytical determination would need to account for all possible angles of collision between anisotropic particles and all iterations of force anisotropy.

An analytical description linking driving force and anisotropy to collision time may enable prediction of critical system densities. Additionally, while the nature of the densest packing in equilibrium can be used to explain the structure seen in dense phase-separated regions, further work is needed to elucidate the link between equilibrium packing and non-equilibrium assembly. As an understanding of the thermodynamics of active matter continues to develop, establishing the phase behavior of active assemblies will be of intense interest as a means of achieving directed, non-equilibrium self-assembly.

While anisotropic active particles are in the early stages with astonishing improvements[38,39] of being synthesized in labs they are ubiquitous in nature. Biology presents us with a number of intriguing test cases for our framework. How does changing shape (as some biological systems are able to do) impact the v/P_{coll} curve? For systems with explicit attractive interactions, e.g. chemotaxis, how can we formulate that interaction as a collision efficiency?

Finally, while our work reveals a mechanism for how particle anisotropy in 2D drives different collective behavior from that seen in disks, our explanation can only describe behavior that we have observed, and is not yet capable of predicting clustering behavior given only a particle anisotropy. Developing a comprehensive predictive theory of how particle anisotropy will impact the critical density would be of great interest to the field.

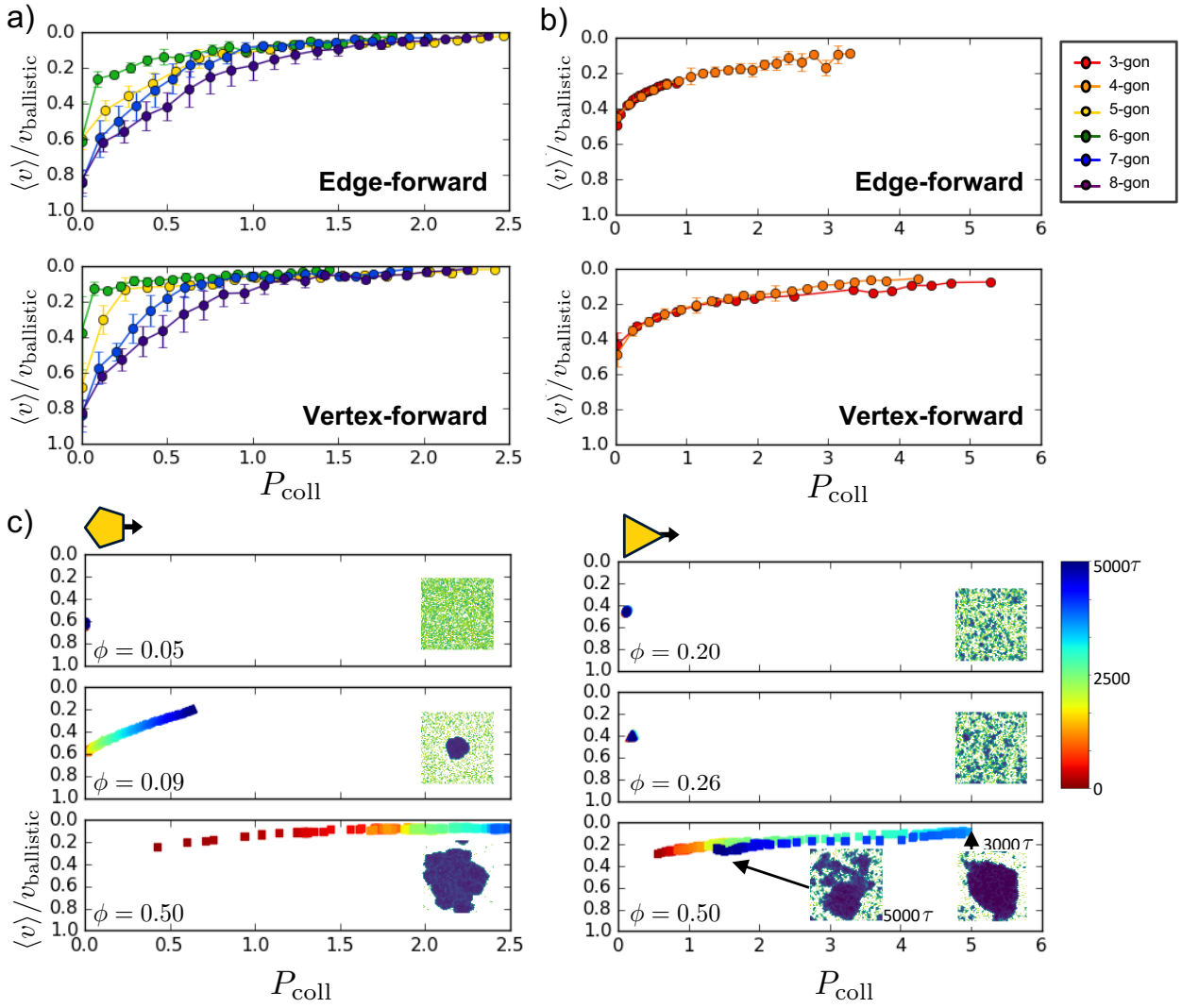

Fig. 6 (a) Shown are the average trajectories for $5 \leq n \leq 8$ in v/P_{coll} space for both edge- and vertex-forward particle simulations. (Note the inverted axis for velocity.) The nucleation, growth, and steady state regions are highlighted. Increasing slope of the growth regime in v/P_{coll} corresponds to decreased ϕ^*, and is predictive for shapes with given force director. Error bars are the standard deviation, with full calculations detailed in Section A.4. Where error bars are not visible, they are smaller than the data marker. (b) Trajectories for 3- and 4-gons are plotted separately. Here, both shapes collapse onto one master curve. The master curves for edge- and vertex-forward 3- and 4-gons also collapse onto on another. Error bars are calculated as in (a). (c) Individual trajectories are shown for 5- and 3-gons at the indicated ϕ. While velocity decreases monotonically with increasing P_{coll} for 5-gons, in 3-gons we observe an "oscillation" in which the largest cluster in the system breaks up at $\phi = 0.50$. Pressure and velocity snapshots are taken every 100τ.

A Appendix

A.1 Simulation protocol

The area fraction covered by N particles was calculated as $\phi = \frac{NA_i}{A_{\text{box}}}$, where the area A_i of particle i includes both the hard shape and the rounding of $r_{\text{WCA}} = 1$ induced by the WCA potential. Each simulation contains $N = 1 \times 10^4$ particles in a square simulation box with periodic boundaries, with box size chosen to achieve the desired density.

The timescale of the simulation, τ, is the time for a particle to ballistically travel its own diameter ($\tau = \frac{\sigma\gamma}{v_0}$). The Langevin equations of motion were numerically integrated using a stepsize of 1×10^{-3}, chosen to balance efficiency with simulation stability. Particle positions were randomly initialized and allowed to relax with a repulsive isotropic potential between particle centroids at $\phi = 0.10$ for 5×10^5 time steps. This isotropic potential was then turned off and the WCA excluded volume potential between particle perimeter points was turned on while the box was slowly compressed to the target system density over 5×10^5 time steps. Only after these initialization steps was the active force turned on and the simulation run for 5000τ.

We assert that the simulations have reached steady state when the total system inter-particle collision pressure has reached a constant value. Ten replicates were run at each statepoint to provide sufficient statistics near the critical density.

Simulations were run using the open-source molecular dynamics software HOOMD-blue (v2.2.1 with CUDA 7.5). The Langevin integrator uses a velocity-Verlet implementation[40]. Simulations were performed on graphics processing units (GPUs)[40,41]. Shape interactions were modeled using the discrete element method implementation in HOOMD-blue[33] using an optimized rigid body routine for particle rotations[41]. The isotropic repulsive potential during initialization was implemented using the dissipative particle dynamics (DPD) pair force implemented in HOOMD-blue[42].

Additional open-source software were used in visualization and analysis. Density and order parameter calculations detailed below were implemented with Freud[43] (`https://github.com/glotzerlab/freud`). Simulation data were visualized using Plato (`https://github.com/glotzerlab/plato`) and Ovito[44]. The structural order color wheel is the color part of the cubehelix[45] colormap at constant apparent luminance ($s = 4$, $r = 1$, $h = 2$, $\gamma = 1$).

A.2 Critical density identification

Multiple methods exist in the literature to determine the critical density for phase separation in active systems. In an active system of squares[22], a system was considered "clustered" if the fraction of system particles in the largest cluster was ≥ 0.2. However, we found this method to be ill-suited for our systems, some of which are comprised of many small clusters. In disks, studies have used local-density histograms about randomly-sampled points of the simulation box[13] or about each particle[10]. If the histogram displayed two peaks, the system was considered phase separated. However, the very low system densities studied here limit the efficacy of the random-sample approach (e.g. at a packing fraction of 0.01, the high-density "peak" would be $\leq 2\%$ of the magnitude of the larger peak). In dumbbells, studies used both a grid-based and Voronoi-based local density calculation to develop local density histograms, to equal effect[46].

To determine phase separation even at low densities, we calculated two separate histograms of local densities within a $2.5r_{\max}$ radius (1) of randomly sampled points ($N = 1 \times 10^5$) and (2) about each particle ($N = 1 \times 10^4$). For each shape, $r_{\max}$ was calculated as the circumscribing radius about the shape. We then calculated a position-normalized local density histogram of the system by multiplying the frequencies of local densities in each local density bin by one another. If the resulting histogram has a high-density peak $\geq 20\%$ the height of the low-density peak, we consider the system to be phase separated. We choose the threshold of 20% to stay consistent with previous studies[22]. However, the high-density peak quickly becomes dominant in the phase separated state such that a different choice would only change our results marginally.

The onset of this phase separation is characterized by a critical particle density, ϕ^*, at which the system transitioned from a homogeneous mixture to coexisting low and high density phases. We define the critical density, ϕ^*, as the lowest density at which $> 50\%$ of the system replicates phase separate. In Figure 2, error bars are given as the range of densities, which have some replicates exhibiting both homogenous and with others exhibiting phase-separating behavior, and indicate an upper and lower limit.

A.3 Structural order in clusters

We examine internal cluster structure with two order parameters. We first calculated the k-atic order parameter, i.e. the bond-orientation order parameter for k-fold rotational symmetry.

$$\psi_k(i) = \frac{1}{n}\sum_j^n e^{ki\theta_{ij}} \tag{3}$$

The parameter k governs the symmetry of the order parameter while the parameter n governs the number of neighbors of particle i to average over. For calculating bond order, θ_{ij} is the angle between the vector r_{ij} and $(1,0)$, i.e. the angle of the bond between particle i and particle j with respect to the x-axis. In other systems, ψ_k has been used to identify hexagonal ($k = 6$) order in systems of active disks[10] and ordering on a square lattice ($k = 4$) in systems of active squares[22].

The body-orientation order parameter tells us relative *orientations* of local particles,

$$\xi_s(j) = e^{is\theta_j} \tag{4}$$

taking into account s-fold symmetry, where θ_j is the angle that rotates particle j from a reference frame into a global coordinate system and i is the imaginary unit. For particles with even n, $s = n$; for particles with odd n, we set $s = 2n$ to account for anti-parallel packings[37].

A.4 Collision pressure calculation

In a 2D system of particles, we used HOOMD (v2.2.1) to calculate the instantaneous (scalar) pressure of the system as $P = (2K + 0.5W)/A$, where K is the total kinetic energy containing thermal and active swimming contributions, W is the configurational component of the pressure virial, and A is the area of the box. We can isolate the pressure due to inter-particle collisions, $W/A = \frac{1}{2A}\sum_i \sum_{j\neq i} \boldsymbol{F}_{ij} \cdot \boldsymbol{r}_{ij} = P - \frac{2K}{A}$. We further normalize the pressure by the thermal energy as $P_{\text{coll}} \equiv (W/A)/k_BT$ to facilitate comparison among systems of particles, as k_BT is varied by shape to maintain constant $\text{Pe} = 150$. While pressure in equilibrium systems is typically taken over an ensemble, here we use it as an instantaneous measure of the location in configuration space of the system. This allows us to view particle trajectories in velocity and configuration space, allowing for the definition of a unique master curve for each system.

To calculate each shape's "trajectory" through v/P_{coll} space shown in Figure 6, we sampled complete simulation trajectories for simulations below, at, and above the critical density, and calculated a distinct P_{coll} and average particle velocity $\langle v \rangle$ for each time step. We then binned the P_{coll} values into equal-size bins, and calculate an overall average $\langle v \rangle$ and standard deviation of $\langle v \rangle$ for each bin. These averages and standard deviations are normalized by the $v_{\text{ballistic}}$ calculated for each shape, and are plotted against the average P_{coll} value in the corresponding bin.

Acknowledgements

The authors thank Matthew Spellings and Chengyu Dai for helpful discussions. This work was supported as part of the Center for Bio-Inspired Energy Science, an Energy Frontier Research Center funded by the U.S. Department of Energy, Office of Science, Basic Energy Sciences under Award #DE-SC0000989. S.E.M. acknowledges support from National Science Foundation Graduate Research Fellowship Grant No. DGE 1256260 and a graduate fellowship from the Association for Computing Machinery Special Interest Group on High Performance Computing and Intel. This research was supported in part through computational resources and services supported by Advanced Research Computing at the University of Michigan, Ann Arbor. This research used resources of the Oak Ridge Leadership Computing Facility, which is a DOE Office of Science User Facility supported under Contract DE-AC05-00OR22725.

Notes and references

1 Sriram Ramaswamy. The mechanics and statistics of active matter. *Annual Review of Condensed Matter Physics*, 1(1):323–345, Aug 2010.

2 M. C. Marchetti, J. F. Joanny, S. Ramaswamy, T. B. Liverpool, J. Prost, Madan Rao, and R. Aditi Simha. Hydrodynamics of soft active matter. *Reviews of Modern Physics*, 85(3):1143–1189, Jul 2013.

3 Clemens Bechinger, Roberto Di Leonardo, Hartmut Löwen, Charles Reichhardt, Giorgio Volpe, and Giovanni Volpe. Active particles in complex and crowded environments. *Reviews of Modern Physics*, 88(4), Nov 2016.

4 M. C. Marchetti, Y. Fily, S. Henkes, A. Patch, and D. Yllanes. Minimal model of active colloids highlights the role of mechanical interactions in controlling the emergent behavior of active matter. *Current Opinion in Colloid & Interface Science*, 21:34–43, 2016.

5 T. Vicsek, E. Czirók, Ben-Jacob, I. Cohen, and O. Shochet. Novel type of phase transition in a system of self-driven particles. *Physical Review Letters*, 75(6), 1995.

6 M. E. Cates, D. Marenduzzo, I. Pagonabarraga, and J. Tailleur. Arrested phase separation in reproducing bacteria creates a generic route to pattern formation. *Proceedings of the National Academy of Sciences*, 107(26):11715–11720, 2010.

7 M. E. Cates and J. Tailleur. When are active brownian particles and run-and-tumble particles equivalent? consequences for motility-induced phase separataion. *Europhysics Letters*, 101(20010), 2013.

8 Yaouen Fily and M. Cristina Marchetti. Athermal phase separation of self-propelled particles with no alignment. *Physical Review Letters*, 108(23), Jun 2012.

9 Gabriel S. Redner, Aparna Baskaran, and Michael F. Hagan. Reentrant phase behavior in active colloids with attraction. *Physical Review E*, 88(1), Jul 2013.

10 Gabriel S. Redner, Michael F. Hagan, and Aparna Baskaran. Structure and dynamics of a phase-separating active colloidal fluid. *Physical Review Letters*, 110(5), Jan 2013.

11 David Richard, H. Loewen, and Thomas Speck. Nucleation pathway and kinetics of phase-separating active brownian particles. *Soft Matter*, 12:5257–5264, 2016.

12 Gabriel S. Redner, Caleb G. Wagner, A. Baskaran, and Michael F. Hagan. Classical nucleation theory description of active colloid assembly. *Physical Review Letters*, 117(148002), 2016.

13 Isaac R. Bruss and Sharon C. Glotzer. Phase separation of self-propelled ballistic particles. *Physical Review E*, 97(042609), 2018.

14 J. Palacci, S. Sacanna, A. P. Steinberg, D. Pine, and P. M. Chaikin. Living crystals of light-activated colloidal surfers. *Science*, 339:936–940, 2013.

15 Alexander P. Petroff, Xiao-Lun Wu, and Albert Libchaber. Fast-moving bacteria self-organize into active two-dimensional crystals of rotating cells. *Physical Review Letters*, 114(15), Apr 2015.

16 G. Briand and O. Dauchot. Crystallization of self-propelled hard discs. *Physical Review Letters*, 117(9), Aug 2016.

17 H. H. Wensink and H. Loewen. Emergent states in dense systems of active rods: from swarming to turbulence. *Journal of Physics: Condensed Matter*, 24(464130), 2012.

18 H. H. Wensink, J. Dunkel, S. Heidenreich, K. Drescher, R. E. Goldstein, H. Lowen, and J. M. Yeomans. Meso-scale turbulence in living fluids. *Proceedings of the National Academy of Sciences*, 109(36):14308–14313, Aug 2012.

19 Yingzi Yang, Vincent Marceau, and Gerhard Gompper. Swarm behavior of self-propelled rods and swimming flagella. *Physical Review E*, 82(3), Sep 2010.

20 H. H. Wensink, V. Kantsler, R. E. Goldstein, and J. Dunkel. Controlling active self-assembly through broken particle-shape symmetry. *Physical Review E*, 89(1), Jan 2014.

21 Sven Erik Ilse, Christian Holm, and Joost de Graaf. Surface roughness stabilizes the clustering of self-propelled triangles. *The Journal of Chemical Physics*, 145(13):134904, Oct 2016.

22 V. Prymidis, S. Samin, and L. Filion. State behaviour and dynamics of self-propelled brownian squares: a simulation study. *Soft Matter*, 2016.

23 M. Aldana, M. Fuentes-Cabrera, and M. Zumaya. Self-propulsion enhances polymerization. *Entropy*, 22(2), 2020.

24 N. H. P. Nguyen, Daphne Klotsa, Michael Engel, and S. C. Glotzer. Emergent collective phenomena in a mixture of hard shapes through active rotation. *Physical Review Letters*, 112(7), Feb 2014.

25 Syeda Sabrina, Matthew Spellings, Sharon C. Glotzer, and Kyle J. M. Bishop. Coarsening dynamics of binary liquids with active rotation. *Soft Matter*, 11(43):8409–8416, 2015.

26 Matthew Spellings, Michael Engel, Daphne Klotsa, Syeda Sabrina, Aaron M. Drews, Nguyen H. P. Nguyen, Kyle J. M. Bishop, and Sharon C. Glotzer. Shape control and compartmentalization in active colloidal cells. *Proceedings of the National Academy of Sciences*, 112(34):E4642–E4650, Aug 2015.

27 A. Suma, G. Gonnella, D. Marenduzzo, and E. Orlandini. Motility-induced phase separation in an active dumbbell fluid.

Europhysics Letters, 108(56004), 2014.

28 Leticia F. Cugliandolo, Pasquale Digregorio, Giuseppe Gonnella, and Antonio Suma. Phase coexistence in two-dimensional passive and active dumbbell systems. *Physical Review Letters*, 119(26), Dec 2017.

29 John D. Weeks, David Chandler, and Hans C. Andersen. Role of repulsive forces in determining the equilibrium structure of simple liquids. *The Journal of Chemical Physics*, 54(12):5237–5247, Jun 1971.

30 Carlos Avendaño and Fernando A. Escobedo. Phase behavior of rounded hard-squares. *Soft Matter*, 8(17):4675, 2012.

31 K. Zhao, R. Bruinsma, and T. G. Mason. Entropic crystal-crystal transitions of brownian squares. *Proceedings of the National Academy of Sciences*, 108(7):2684–2687, Jan 2011.

32 Kun Zhao and Thomas G. Mason. Frustrated rotator crystals and glasses of brownian pentagons. *Physical Review Letters*, 103(20), Nov 2009.

33 Matthew Spellings, Ryan L. Marson, Joshua A. Anderson, and Sharon C. Glotzer. Gpu accelerated discrete element method (dem) molecular dynamics for conservative, faceted particle simulations. *Journal of Computational Physics*, 334:460–467, 2017.

34 Robin van Damme, Jeroen Rodenburg, RenÃ© van Roij, and Marjolein Dijkstra. Interparticle torques suppress motility-induced phase separation for rodlike particles. *The Journal of Chemical Physics*, 150(16):164501, 2019.

35 Previous studies find slightly different critical behavior than we find here. **3-gons:** Very rounded approximations of our edge and vertex forward triangles were able to slide by one another like disks, leading to different phase behavior than we observe (e.g. laning)[20]. In a study of triangles with additional steric interactions due to a rigid-body construction of disks approximating fricitons, vertex-forward simulations also cluster more efficiently than edge-forward triangles, but no quantitative explanation was offered for the oscillatory behavior observed[21]. **4-gons**: The critical density we find for 4-gons is higher than that found in a previous work[22]. This is likely due to two key differences between their methods and ours. First, they set their cut-off for phase separation as the regime where the largest cluster fraction remains higher than 10%, a lower threshhold than we use here. Second, their squares are slightly less round than ours, which we would expect to lead to a lower critical density.

36 Yan Liu, Yuguang Yang, Bo Li, and Xi-Qiao Feng. Collective oscillation in dense suspension of self-propelled chiral rods. *Soft Matter*, 15:2999–3007, 2019.

37 Steven Atkinson, Yang Jiao, and Salvatore Torquato. Maximally dense packings of two-dimensional convex and concave noncircular particles. *Physical Review E*, 86(3), Sep 2012.

38 R. P. Doherty, T. Varkevisser, M. Teunisse, J. Hoecht, S. Ketzetzi, S. Ouhajji, and D. J. Kraft. Catalytically propelled 3d printed colloidal microswimmers. *Soft Matter*, 16:10463–10469, 2020.

39 Z. Wang, W. Xu, Z. Wang, D. Lyu, Y. Mu, W. Duan, and Y. Wang. Polyhedral micromotors of metal–organic frameworks: Symmetry breaking and propulsion. *Journal of the American Chemical Society*, 2021.

40 Joshua A. Anderson, Chris D. Lorenz, and A. Travesset. General purpose molecular dynamics simulations fully implemented on graphics processing units. *Journal of Computational Physics*, 227(10):5342–5359, May 2008.

41 Jens Glaser, Trung Dac Nguyen, Joshua A. Anderson, Pak Lui, Filippo Spiga, Jaime A. Millan, David C. Morse, and Sharon C. Glotzer. Strong scaling of general-purpose molecular dynamics simulations on gpus. *Computer Physics Communications*, 192:97–107, 2015.

42 Carolyn L. Phillips, Joshua A. Anderson, and Sharon C. Glotzer. Pseudo-random number generation for brownian dynamics and dissipative particle dynamics simulations on gpu devices. *Journal of Computational Physics*, 230(19):7191–7201, Aug 2011.

43 Vyas Ramasubramani, Bradley D. Dice, Eric S. Harper, Matthew P. Spellings, Joshua A. Anderson, and Sharon C. Glotzer. freud: A software suite for high throughput analysis of particle simulation data, 2019.

44 Alexander Stukowski. Visualization and analysis of atomistic simulation data with OVITO-the Open Visualization Tool. *MODELLING AND SIMULATION IN MATERIALS SCIENCE AND ENGINEERING*, 18(1), JAN 2010.

45 D. A. Green. A colour scheme for the display of astronomical intensity images, 2011.

46 Isabella Petrelli, Pasquale Digregorio, Leticia F. Cugliandolo, Giuseppe Gonnella, and Antonio Suma. Active dumbbells: Dynamics and morphology in the coexisting region. *The European Physical Journal E*, 41(10):128, Oct 2018.